Acta Crystallographica Section D
Biological Crystallography
ISSN 0907-4449

Structure of a crystal form of human methemoglobin indicative of fiber formation

Steven B. Larson,[a] John S. Day,[a] Chieugiang Nguyen,[b] Robert Cudney[b] and Alexander McPherson[a]*

[a]Department of Molecular Biology and Biochemistry, University of California, Irvine, CA 92697-3900, USA, and [b]Hampton Research, 34 Journey, Aliso Viejo, CA 92656-3317, USA

Correspondence e-mail: amcphers@uci.edu

Received 17 August 2010
Accepted 8 October 2010

PDB Reference:
methemoglobin, 3odq.

Human methemoglobin was crystallized in a unique unit cell and its structure was solved by molecular replacement. The hexagonal unit cell has unit-cell parameters $a = b = 54.6$, $c = 677.4$ Å, with symmetry consistent with space group $P6_122$. The unit cell has the second highest aspect ratio of all unit cells contained in the PDB. The 12 molecules in the unit cell describe a right-handed helical filament having no polarity, which is different from the filament composed of HbS fibers, which is the only other well characterized fiber of human hemoglobin. The filaments reported here can be related to canonical sickle-cell hemoglobin filaments and to an alternative sickle-cell filament deduced from fiber diffraction by slight modifications of intermolecular contacts.

1. Introduction

In the course of our investigations on the propensity of certain small molecules to promote macromolecular crystallization (McPherson & Cudney, 2006; Larson *et al.*, 2007), we grew crystals of human hemoglobin in a number of trials. The hemoglobin, which was rust in color, possessed an absorption spectrum that indicated it to be in the met form. Ferricyanide-treated protein, which yields methemoglobin (Magos, 1964), yielded the same crystals. As we describe below, the crystal structure is noteworthy. The crystallographic unit cell has the second highest aspect ratio of any contained in the PDB and the structure implies that the hexagonal crystals are composed of filaments of methemoglobin molecules lying parallel to the *c* axis.

Methemoglobin does not bind oxygen, but neither is it reported to assume the quaternary arrangement of deoxyhemoglobin. This is significant because it is deoxyhemoglobin that forms fibers of sickle-cell hemoglobin as a consequence of the mutation of glutamic acid at position 6 of the β chain in normal human hemoglobin to valine in the sickle-cell protein. There is, however, at least one previous report of nonsickle hemoglobin forming fibers and this report may be pertinent to the fibers we describe here. Finch *et al.* (1973) noted that

> similar filaments [to those seen in sickled cells] are also observed in normal deoxygenated erythrocytes, but in much lower concentration, and aggregated into fibers of irregular diameter.

A second report suggesting the existence of alternate hemoglobin filament forms comes from a study of sickle-cell fibers by Mu & Magdoff-Fairchild (1992). They observed a second filament form that was clearly different from the

Table 1
Data-processing, refinement and model statistics.

Values in parentheses are for the highest resolution shell.

Crystal data	
Space group	$P6_122$
Z	12
Unit-cell parameters (Å)	$a = b = 54.60$, $c = 677.42$
Data-processing statistics	
Resolution (Å)	47.29–2.60 (3.21–2.60)
No. of reflections	17172
Multiplicity	8.13 (2.65)
$\langle I/\sigma(I)\rangle$	7.2 (1.3)
Completeness (%)	85.0 (39.6)
$R_{\rm merge}$†	0.131 (0.562)
Structure-refinement statistics	
Resolution (Å)	3.1
No. of reflections [$F_o = 0$ removed]	11863 [96.6%]
$R/R_{\rm free}$‡ [$F > 0\sigma(F)$]	0.284/0.325
% in test set	4.9
Model statistics	
Protein atoms	4384
Heme atoms	172
Geometry: r.m.s. deviations from ideal values	
Bonds (Å)	0.024
Angles (°)	2.00
Average isotropic B factors (Å^2)	170
Ramachandran plot	
Most favored region	456 [91.6%]
Allowed region	42 [8.4%]
Generously allowed and disallowed regions	0

† $R_{\rm merge} = \sum_{hkl}\sum_i |I_i(hkl) - \langle I(hkl)\rangle|/\sum_{hkl}\sum_i I_i(hkl)$, where $I_i(hkl)$ is the ith used observation for unique hkl and $\langle I(hkl)\rangle$ is the mean intensity for unique hkl. ‡ $R = \sum_{hkl}||F_{\rm obs}| - |F_{\rm calc}||/\sum_{hkl}|F_{\rm obs}|$, where $F_{\rm obs}$ and $F_{\rm calc}$ are the observed and calculated structure-factor amplitudes, respectively.

'classical' filament and consisted of a single rather than a double strand of hemoglobin molecules. Their model for this alternate filament was based on X-ray fiber diffraction data obtained from a sample of sickle-cell hemoglobin fibers that had been left standing in an X-ray capillary for a long period of time. The data were recorded from a single region of the capillary that was immediately adjacent to a region that contained microcrystals (representing another transformation) and a second region which contained fibers yielding diffraction patterns consistent with the 'classical' HbS fibers. The implication of their results was that the 'classical' HbS filaments could transform in time to a filament of different structure.

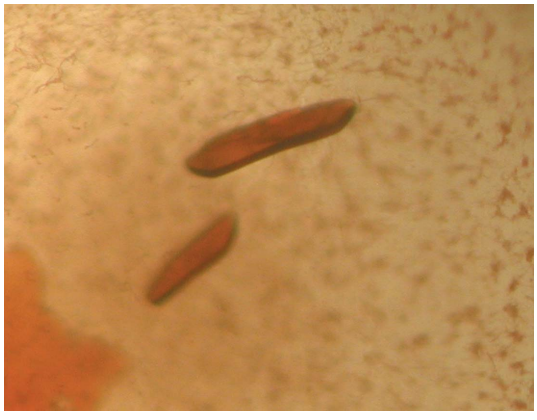

Figure 1
Crystals of human methemoglobin grown at pH 5.5 from 25%(*w*/*v*) polyethylene glycol 3350 at 298 K.

2. Experimental procedures

Human hemoglobin was purchased from Sigma Biochemical Co. (St Louis, Missouri, USA) and was used without further purification or treatment. It was dissolved in water to a concentration of 30 mg ml^{-1} and clarified by centrifugation. An array of experimental crystallization conditions were deployed in an attempt to reproducibly grow crystals. This was carried out using vapor diffusion in Cryschem plates (Hampton Research, Aliso Viejo, California, USA) with drops of 4–6 µl volume. Some success was obtained in that crystals could be predictably grown from 15–30% PEG buffered at pH 4.5–5.5 in the presence of 0.2 *M* salt of several varieties. Most crystals were too small or too fragile to be of use for X-ray diffraction or grew in clusters. Some, however, were adequate. Two dimensions presented no obstacle, although growth in the third dimension was problematic. A typical example of the crystals is shown in Fig. 1. The crystals were red plates of 0.2–0.4 mm on edges, but perhaps no more than 20 µm thick.

Crystals were mounted in loops, immediately flash-frozen in their mother liquor and shipped to SSRL for remote data collection on beamline 7-1. Preliminary diffraction patterns were obtained that showed reflections to be resolved along all

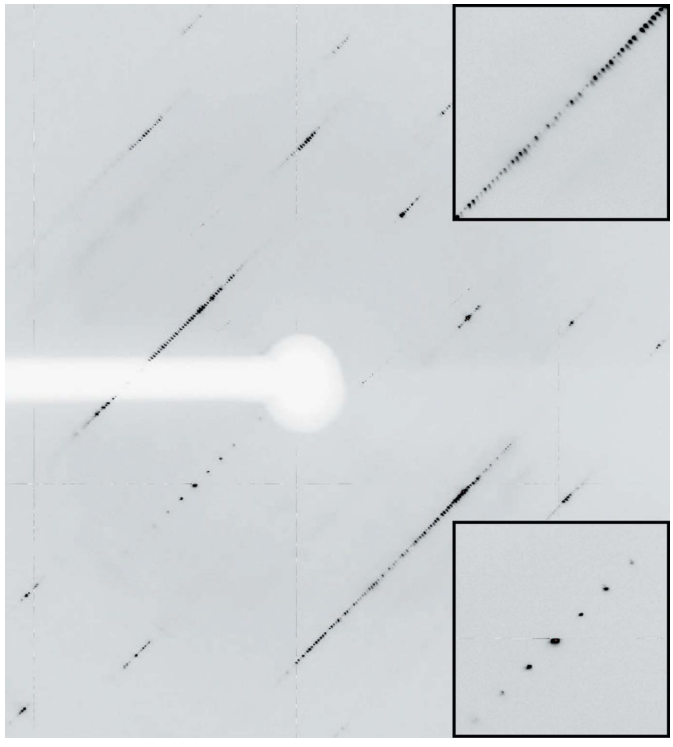

Figure 2
Diffraction image obtained on SSRL beamline 7-1. A detail showing the resolution of the reflections along the 677.4 Å axis is shown at the top right. A detail showing the 00*l* line of reciprocal space and the presence of only reflections for which $l = 6n$ is shown at the bottom right. The images are from *d*TREK* (Pflugrath, 1999).

axes. An example is presented in Fig. 2. A preliminary 4.5 Å resolution X-ray diffraction data set was collected from which the crystal structure was solved by molecular replacement. Subsequently, two crystals that diffracted to higher resolution were obtained, data from which were collected on SSRL beamline 9-2, processed and merged to 2.6 Å resolution. Scan widths of 0.33° and 0.50° and exposure times ranging from 9 to 60 s were used. The mosaicities of the crystals were 0.52° and 0.80°, respectively. For data processing and merging we used the program *d*TREK* (Pflugrath, 1999). Table 1 presents the data-collection statistics. As described below, structure solution was attempted using both *CNS* (Brünger *et al.*, 1998) and *Phaser* (McCoy *et al.*, 2005) and several search models. Refinement was carried out using *CNS*, graphical analysis employed the program *Coot* (Emsley & Cowtan, 2004) and presentation figures were made using *PyMOL* (DeLano, 2002).

3. Results

The crystals used for model refinement had hexagonal unit-cell parameters of $a = b = 54.6$, $c = 677.4$ Å, although c axes in the range 672–682 Å were observed for different samples. The diffraction image of Fig. 2 captures the 00l line of reciprocal-lattice points, which indicated the presence of only those reflections having $l = 6n$. Analysis of the full three-dimensional data set confirmed the systematic absences as well as the presence of mirror planes parallel to c. The space group was therefore $P6_122$ (or $P6_522$).

Comparison with other hemoglobin crystals in the PDB (Berman *et al.*, 2000) and calculation of the volume-to-mass ratio of the crystal (2.3 Å^3 Da^{-1}; Matthews, 1968) indicated that the asymmetric unit consisted of an entire hemoglobin molecule (one $\alpha_2\beta_2$ tetramer). The unit cell is unusual in its aspect ratio, being the second highest in the PDB. The symmetry and dimensions suggested that the protein had crystallized in the form of continuous helical filaments having 6_122 (or 6_522) symmetry, a periodicity of 677 Å and 12 hemoglobin molecules per turn of the helix.

Attempts to solve the structure by molecular replacement using *CNS* (Brünger *et al.*, 1998) in either possible space group and with several probe models of normal human hemoglobin gave no clear solution. We considered the possibility that the crystals were merohedrally twinned, in which case the true space group could be $P6_1$ or $P6_5$. However, the test for twinning (Yeates, 1997) was ambiguous, with the statistics for the lower resolution data suggesting no twinning and those for the higher resolution data suggesting that there might be twinning. Efforts to solve the structure with the assumption of twinning led nowhere.

A search using human sickle-cell hemoglobin (PDB entry 1nej; Patskovska *et al.*, 2005) as the search model, however, gave a single prominent solution (with *Phaser*) in space group $P6_122$. A retrospective examination of earlier failed attempts to obtain a molecular-replacement solution with other probes using *CNS* showed that the correct solution was frequently present among other possibilities but could not be discriminated from incorrect solutions. With the prominent solution given by sickle-cell hemoglobin, the molecules were closely packed but with virtually no unacceptable contacts. The initial R factor after molecular replacement and rigid-body refinement against our preliminary data was 0.38 ($R_{\rm free}$ = 0.49) at 4.5 Å resolution.

Since the binding of oxygen to hemoglobin is accompanied by a rotation of one $\alpha\beta$ heterodimer with respect to the other $\alpha\beta$ dimer, we calculated the rotation of our model with respect to the deoxyhemoglobin model PDB entry 2dn2. The value of 15° was similar to that obtained for the 1.25 Å carbonmonoxyhemoglobin model PDB entry 2dn3. Therefore, the 2dn3 model was superimposed on our refined 1nej model and

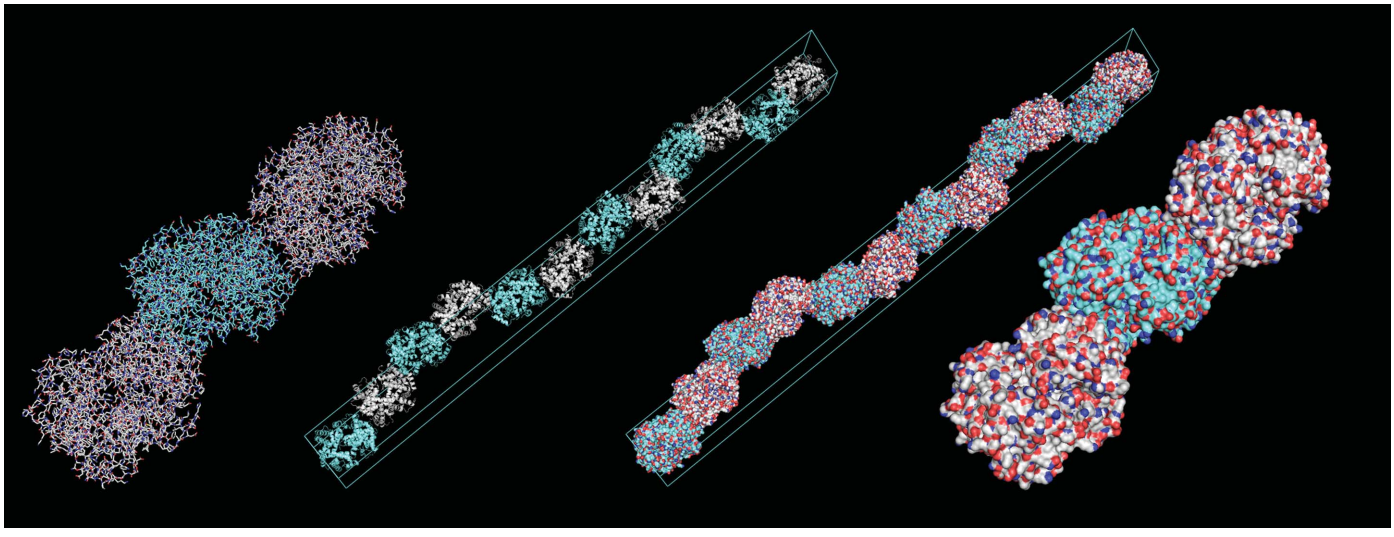

Figure 3
The contents of the hexagonal unit cell and the filament that it defines are shown in ribbon and surface representations in the center, along with an outline of the unit cell for reference. Details consisting of three hemoglobin molecules and the two kinds of interfaces that relate them are shown on the far left and far right. The filaments display 6_122 symmetry with a periodicity of 677.5 Å.

refinement of this new model, which had the correct sequence and represented a higher resolution starting model, was continued against the higher resolution data. It should be noted here that the initial $\alpha\beta$ dimer rotation for model 1nej was 22° and refinement reduced the angle to the 15° mentioned above, which is similar to the values observed for met-HbA and ten models of oxy-HbA and carbonmonoxy-HbA.

A series of one-body, two-body, four-body and eight-body rigid-body refinements followed by side-chain and *B*-factor refinement and a final refinement in which the backbone atoms were harmonically restrained were performed using *CNS* at various resolutions from 3.2 to 2.6 Å in 0.1 Å increments. The rigid groups were defined as follows: the one-body group was the whole molecule, the two-body groups were the $\alpha\beta$ heterodimers (including their associated heme groups) that rotate with respect to each other when oxygen binds, the four-body groups were the individual chains with associated heme groups and the eight-body groups were the four protein chains and the four heme groups. The models and maps lacked clarity; the temperature factors were high and the maps were reminiscent of lower resolution maps. Because of the marginal quality of the density, it seemed most prudent to limit refinement to the harmonically restrained models. Attempts to refine positional parameters without harmonic restraints, while decreasing the *R* factor and improving the r.m.s. deviations in bonds and angles, resulted in a significant increase in $R_{\rm free}$. The model reported here and deposited in the Protein Data Bank was refined at a resolution of 3.1 Å and had the lowest $R_{\rm free}$ of all the models obtained from the aforementioned series of refinements. Refinement and model statistics are presented in Table 1. Because of the very restrained refinement protocol used for the final model, the molecular geometry, as defined by r.m.s. deviations in bonds and angles, are very similar to the 1.25 Å starting model. The high *B* factors suggest that there is disorder on the molecular level, not just on the atomic level. There may be multiple quaternary structures of the hemoglobin molecules or a single quaternary structure with multiple orientations at each molecular site in the crystal lattice. However the disorder occurs, we are confident in our solution of the crystal structure and the molecular interfaces that are observed since they have been observed in other hemoglobin structures as discussed below.

The contents of a unit cell are shown in Fig. 3 and these repeat along *c* at 677.4 Å intervals to form helical filaments that run continuously through the crystal. Each molecule of hemoglobin shares an interface with a molecule ahead and a molecule behind. The two interfaces are different: one is produced by the 6_1 screw operation and the other contains a twofold crystallographic axis perpendicular to the helical axis. The former interface, produced by the screw operation, chiefly involves polypeptide segments $\beta5$–$\beta17$ of one molecule and $\alpha114$–$\alpha118$, $\beta19$–$\beta26$ and $\beta116$–$\beta117$ of the second. Near the center of the interface is one of the two β-Glu6 residues present in the molecule. This is the amino acid that is mutated to valine in sickle-cell hemoglobin. The latter interface is created by three polypeptide segments contributed by each of the two molecules related by a crystallographic dyad. These are $\beta17$–$\beta22$, $\beta50$–$\beta61$ and $\alpha112$–$\alpha120$. The buried surface area (Lee & Richards, 1971; Brünger *et al.*, 1998) of the first interface is estimated to be 890 Å^2 and that of the second interface is estimated to be 1140 Å^2. Both of the interface areas are well within the ranges associated with protein interfaces responsible for oligomer formation and substantially exceed those normally observed as a consequence of crystal lattice contacts only (Dasgupta *et al.*, 1997). By virtue of the 6_1 axis, the filaments are in the form of a right-handed helix; because of the crystallographic twofold axes, they have no polarity.

We analyzed representatives of the various space groups and unit cells of the human hemoglobin crystal structures present in the PDB and examined all interfaces between molecules in the lattices of these crystals. There were 37 interfaces that exceeded 600 Å^2 in excluded surface area. One of these, of area 973 Å^2, was that found in monoclinic crystals of sickle-cell hemoglobin (PDB entry 2hbs; Harrington *et al.*, 1997) relating two independent molecules in the asymmetric unit (related by a pseudo-2_1 axis), which contains β-Val6 and serves as the basis for the 'classical model' of the sickle-cell hemoglobin filament (Wishner *et al.*, 1975; Padlan &Love, 1985; Carragher *et al.*, 1988). A second major interface of 640 Å^2 of buried surface area was present in orthorhombic crystals of sickle-cell hemoglobin (PDB entry 1nej; Patskovska *et al.*, 2005). This interface corresponds to the interface

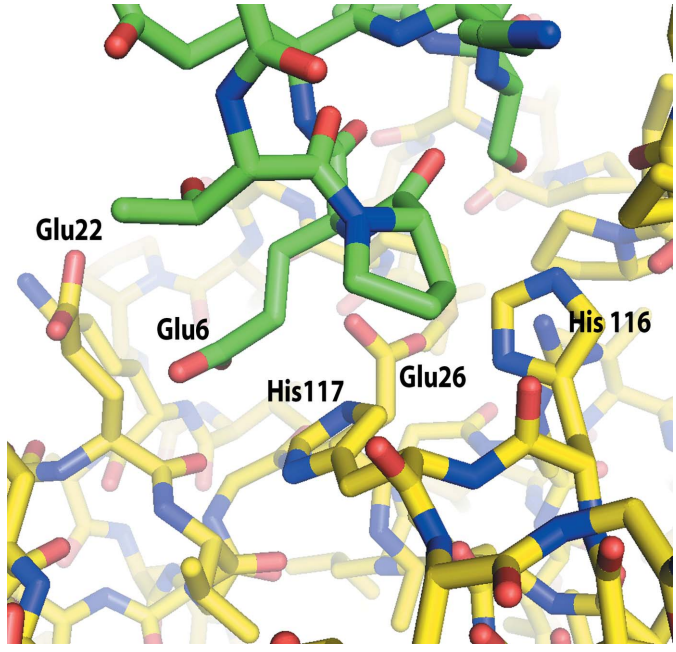

Figure 4
The interface between hemoglobin molecules produced by the 6_1 screw operation (not containing a crystallographic dyad axis). β-Glu6 of one molecule is noted. Its side-chain carboxyl group is near the β-Glu26 and β-Glu22 carboxylate groups of the second molecule. Also nearby are the imidazole side groups of β-His116 and β-His117. The distances are such that at pH 5.5 favorable electrostatic interactions would be established between β-Glu6 of the first molecule and either or both of the histidines of the second molecule.

produced by the 6_1 screw operation (also a 2_1 screw operator) in the 6_122 filaments. A third major interface with an excluded surface area of 1544 Å^2 is seen in the trigonal crystal form of normal hemoglobin (PDB entry 1qxe; Safo *et al.*, 2004) and is nearly identical to the second interface present in the 6_122 filaments that contains the crystallographic twofold axis. The finding that the two interfaces in our structure deduced by molecular replacement are the same as two of the major interfaces previously observed to exist in crystals of human hemoglobin further confirms the molecular-replacement solution.

4. Discussion

4.1. The dyad interface

The interface produced by the 6_1 screw axis along the filament, we feel, is worthy of some attention. Hexagonal crystals of human methemoglobin grow increasingly well as the pH is lowered from neutrality and the optimum seems to be about pH 5.5. The interface, which is seen in Fig. 4, contains β-Glu6, as we noted, but close to its carboxyl group is the carboxyl group of Glu26 from the opposite molecule and, a bit further away, the carboxyl group of Glu22 as well. Within a few angstroms of the β-Glu6 carboxyl are the imidizole rings of histidines β116 and β117, also from the second molecule. The pK_a of glutamate is about 4.25 and that of histidine is 6.0. At physiological pH, the glutamate carboxyls would carry negative charges and set up a repulsive interaction at the interface. The histidine side chains would carry no charge. At pH 5.5, however, the majority of glutamate carboxyls would still carry negative charges, but the positive charges acquired by the histidine side chains would not only neutralize them but would also be likely to establish an attractive interaction between the two protein molecules. At neutral pH the filaments we observe would have difficulty forming, but at acid pH their formation is facilitated. Were β-Glu6 mutated to valine, as it is in HbS, there would be no electrostatic repulsion at any pH and, one supposes, the filaments might then form even at physiological pH.

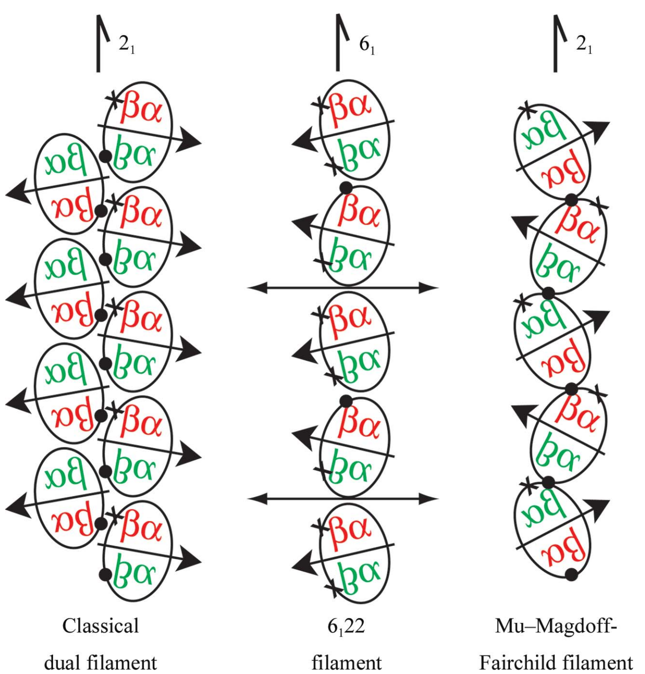

Figure 5
A schematic diagram showing the arrangement of tetrameric hemoglobin molecules in the 'classical' dual filament on the left, the 6_122 filament in the center and the model for a filament proposed by Mu and Magdoff-Fairchild on the right. The filaments can be transformed from one to another by relatively minor changes of the orientations of the molecules comprising the filaments, although the interfaces between molecules in each filament are different as a consequence. The red and green colors represent opposite sides of the α and β chains (to illustrate symmetry). The solid dots represent the positions of β-Glu6 (or β-Val6) residues and the 'hydrophobic pockets' are represented by ×.

4.2. Comparison with 'classical' sickle-cell filaments

The 6_122 filament is clearly different from the model of the 'classical' sickle-cell hemoglobin filament, which has consecutive molecules related by simple translation along a filament (Wishner *et al.*, 1975; Padlan & Love, 1985). In addition, this model has two such filaments related by a 2_1 screw axis, so that the fundamental unit is not a single strand but a double strand of two filaments. The current model for the fiber responsible for sickling consists of seven pairs of filaments (14 filaments in total) forming a helical array of very long period (Dykes *et al.*, 1979; Carragher *et al.*, 1988). Two filaments within the pair are associated through the interaction of β-Val6 with a 'hydrophobic pocket' in a 2_1-related molecule formed by amino acids Ala70, Asp73, Thr84, Phe85 and Leu88 of the other β chain. It is the mutation of β-Glu6 to β-Val6 that permits this interaction to form and thereby promotes filament dimer formation. The mutation does not explain the aggregation of filament dimers into fibers, however, since the second β-Val6 in each protein molecule is rendered inaccessible by the model and is therefore unavailable for lateral interactions between filament dimers within a fiber.

On the left in Fig. 5 is shown a schematic diagram of the 'classical' dual filament model presumed to be the fundamental component of the sickle-cell hemoglobin fibers. In the center and on the right, respectively, are the 6_122 filament and an alternative filament model (see below) described by Mu & Magdoff-Fairchild (1992). Although superficially the three models appear to be rather different, they have some important similarities, principally because a tetrameric hemoglobin molecule contains a molecular twofold axis relating $\alpha\beta$ subunit pairs and in all models these molecular dyads are close to perpendicular to the filament axis. The angle is 9° in the 'classical' dual filament, 13° in the 6_122 filament and about 27° in the Mu–Magdoff-Fairchild model.

As is evident from Fig. 5, when molecular symmetry is considered, the 6_122 fiber when 'straightened out' is simply half of the 'classical' dual filament. To transform the dual fiber into the 6_122 fiber, it is necessary to rotate the molecules slightly in one filament of the pair such that the 'side-to-side' inter-filament interactions involving Val6 are broken (the 2_1

axis is split) as the strand is twisted to follow a course around a 6_1 axis. New interfaces are formed, half of which utilize the amino acid at position 6, with alternate interfaces that do otherwise.

4.3. Possible relationship of the methemoglobin fibers to sickle-cell hemoglobin fibers

It has been noted that sickle-cell hemoglobin fibers are frequently polymorphic (Finch *et al.*, 1973; Ohtsuki *et al.*, 1977; Magdoff-Fairchild & Chiu, 1979; Kaperonis *et al.*, 1986; Mu & Magdoff-Fairchild, 1992; Wang *et al.*, 2000), which suggests that the fiber structure may be variable or ill-defined or that it consists of more than one component. There is also evidence that structural transformations may occur in the filaments making up sickle fibers as a consequence of time or other physical factors (Magdoff-Fairchild & Chiu, 1979; Kaperonis *et al.*, 1986; Mu & Magdoff-Fairchild, 1992).

The Mu–Magdoff-Fairchild result is pertinent because it demonstrated that the 'classical' HbS filaments could transform to yield a fiber diffraction pattern consistent with their model, that seen on the right in Fig. 5. We believe it to be likely that the proper model to explain the diffraction pattern that they recorded may not be that which they proposed, but the 6_122 filament. Indeed, although the Mu–Magdoff-Fairchild model is not the same as the 6_122 filament structure, it is not in fact so very different. Their model can be readily adjusted to be virtually the same as the 6_122 filament. The molecular dyads need be rotated closer to perpendicular to the filament axis (as they would be if the strand were coiled about a 6_1 axis) and every other molecule in the Mu–Magdoff-Fairchild model would require an approximate 180° rotation 'in place' about the direction of the filament axis.

The Mu–Magdoff-Fairchild model was based on low-resolution fiber diffraction data. We would comment in passing that it is unlikely that the resolution of the fiber diffraction patterns would have permitted discrimination between the Mu–Magdoff-Fairchild model and the 6_122 fiber. In any case, their principal objective was to explain the loss of the layer line pertaining to a 64 Å repeat which is present in diffraction patterns from the 'classical' filaments and the appearance of a layer line pertaining to a 109 Å periodicity in their 'new' pattern. To produce a model reflecting those properties, they used the simple expedient of compressing the two filaments of the 'classical' dual strands laterally so that they interleaved and merged along the 2_1 axis. This would eliminate the 64 Å repeat layer line from the fiber diffraction pattern. In addition, the molecules were rotated with respect to one another to re-establish the interaction involving β-Val6. The clever aspect of the Mu–Magdoff-Fairchild model was that the rotation also lengthened the repeat distance along the filament, so that a layer line representing a periodicity of 109 Å would be expected in the diffraction pattern. The axial repeat along the fiber axis in the 6_122 fiber is 111 Å, which is the same within experimental error given the differences in solution (mother-liquor) conditions. We further note that if the helical 6_122 filament were straightened out into a line, as in the 'classical' model, it too would give a strong 64 Å meridonial layer line (54.5 Å/sin 60°). Indeed, the strong second-order meridional reflection in the diffraction pattern from the sickle-cell hemoglobin fibers was the only significant discrepancy that they could not account for in terms of the 'classical' filament.

A possibility consistent with the observed polymorphism of sickle-cell fibers is that they may be composed of filaments having more than one structure. If, for example, the fibers contain the 'classical' filaments and the 6_122 filaments, then both the observed first-order and second-order fiber diffraction intensities would be expected.

Mu and Magdoff-Fairchild offered no explanation as to why the fiber transformation occurred, but noted that it occurred only after a long period of storage in a capillary. Hemoglobin transforms with time quite readily from its normal form to methemoglobin. It seems possible that the deoxy sickle hemoglobin composing the fibers in their capillary did just that. If so, then it seems plausible that the 'classical' sickle-cell hemoglobin fibrils studied by Mu and Magdoff-Fairchild may have transformed into the methemoglobin fibrils we find in our crystals. Finally, it is also possible that the hemoglobin fibers observed by Finch and coworkers in normal deoxygenated red blood cells (Finch *et al.*, 1973) might be the same as the methemoglobin fibers that we describe here.

References

Berman, H. M., Westbrook, J., Feng, Z., Gilliland, G., Bhat, T. N., Weissig, H., Shindyalov, I. N. & Bourne, P. E. (2000). *Nucleic Acids Res.* **28**, 235–242.

Brünger, A. T., Adams, P. D., Clore, G. M., DeLano, W. L., Gros, P., Grosse-Kunstleve, R. W., Jiang, J.-S., Kuszewski, J., Nilges, M., Pannu, N. S., Read, R. J., Rice, L. M., Simonson, T. & Warren, G. L. (1998). *Acta Cryst.* D**54**, 905–921.

Carragher, B., Bluemke, D. A., Gabriel, B., Potel, M. J. & Josephs, R. (1988). *J. Mol. Biol.* **199**, 315–331.

Dasgupta, S., Iyer, G. H., Bryant, S. H., Lawrence, C. E. & Bell, J. A. (1997). *Proteins*, **28**, 494–514.

DeLano, W. L. (2002). *PyMOL.* http://www.pymol.org.

Dykes, G. W., Crepeau, R. H. & Edelstein, S. J. (1979). *J. Mol. Biol.* **130**, 451–472.

Emsley, P. & Cowtan, K. (2004). *Acta Cryst.* D**60**, 2126–2132.

Finch, J. T., Perutz, M. F., Bertles, J. F. & Döbler, J. (1973). *Proc. Natl Acad. Sci. USA*, **70**, 718–722.

Harrington, D. J., Adachi, K. & Royer, W. E. Jr (1997). *J. Mol. Biol.* **272**, 398–407.

Kaperonis, A. A., Handley, D. A. & Chien, S. (1986). *Am. J. Hematol.* **21**, 269–275.

Larson, S. B., Day, J. S., Cudney, R. & McPherson, A. (2007). *Acta Cryst.* D**63**, 310–318.

Lee, B. & Richards, F. M. (1971). *J. Mol. Biol.* **55**, 379–400.

Magdoff-Fairchild, B. & Chiu, C. (1979). *Proc. Natl Acad. Sci. USA*, **76**, 223–226.

Magos, L. (1964). *Biochim. Biophys. Acta*, **90**, 55–61.

Matthews, B. W. (1968). *J. Mol. Biol.* **33**, 491–497.

McCoy, A. J., Grosse-Kunstleve, R. W., Storoni, L. C. & Read, R. J. (2005). *Acta Cryst.* D**61**, 458–464.

McPherson, A. & Cudney, B. (2006). *J. Struct. Biol.* **156**, 387–406.

Mu, X.-Q. & Magdoff-Fairchild, B. (1992). *Biophys. J.* **61**, 1638–1646.

Ohtsuki, M., White, S. L., Zeitler, E., Wellems, T. E., Fuller, S. D., Zwick, M., Makinen, M. W. & Sigler, P. B. (1977). *Proc. Natl Acad. Sci. USA*, **74**, 5538–5542.
Padlan, E. A. & Love, W. E. (1985). *J. Biol. Chem.* **260**, 8272–8279.
Patskovska, L. N., Patskovsky, Y. V., Almo, S. C. & Hirsch, R. E. (2005). *Acta Cryst.* D**61**, 566–573.
Pflugrath, J. W. (1999). *Acta Cryst.* D**55**, 1718–1725.
Safo, M. K., Abdulmalik, O., Danso-Danquah, R., Burnett, J. C., Nokuri, S., Joshi, G. S., Musayev, F. N., Asakura, T. & Abraham, D. J. (2004). *J. Med. Chem.* **47**, 4665–4676.
Wang, Z., Kishchenko, G., Chen, Y. & Josephs, R. (2000). *J. Struct. Biol.* **131**, 197–209.
Wishner, B. C., Ward, K. B., Lattman, E. E. & Love, W. E. (1975). *J. Mol. Biol.* **98**, 179–194.
Yeates, T. O. (1997). *Methods Enzymol.* **276**, 344–358.